Harnessing Dispersion in Soliton Microcombs to Mitigate Thermal Noise

Jordan R. Stone[1,2,*] and Scott B. Papp[1,2]
[1]*Time and Frequency Division, National Institute for Standards and Technology, Boulder, Colorado 80305, USA*
[2]*Department of Physics, University of Colorado Boulder, Boulder, Colorado 80309, USA*

(Received 26 May 2020; revised 17 August 2020; accepted 8 September 2020; published 5 October 2020)

We explore intrinsic thermal noise in soliton microcombs, revealing thermodynamic correlations induced by nonlinearity and group-velocity dispersion. A suitable dispersion design gives rise to control over thermal-noise transduction from the environment to a soliton microcomb. We present simulations with the Lugiato-Lefever equation (LLE), including temperature as a stochastic variable. By systematically tuning the dispersion, we suppress repetition-rate frequency fluctuations by up to 50 decibels for different LLE soliton solutions. In an experiment, we observe a measurement-system-limited 15-decibel reduction in the repetition-rate phase noise for various settings of the pump-laser frequency, and our measurements agree with a thermal-noise model. Finally, we compare two octave-spanning soliton microcombs with similar optical spectra and offset frequencies, but with designed differences in dispersion. Remarkably, their thermal-noise-limited carrier-envelope-offset frequency linewidths are 1 MHz and 100 Hz, which demonstrates an unprecedented potential to mitigate thermal noise. Our results guide future soliton-microcomb design for low-noise applications, and, more generally, they illuminate emergent properties of nonlinear, multimode optical systems subject to intrinsic fluctuations.

DOI: 10.1103/PhysRevLett.125.153901

Optical-frequency combs are powerful and versatile tools for making precision measurements across the electromagnetic spectrum [1]. To reach applications outside the laboratory, integrated-photonics frequency combs based on continuous-wave (CW) laser-pumped microresonator solitons are rapidly being advanced [2]. Microresonators simultaneously achieve high quality factor (Q) and small mode volume (V) to intensify the intraresonator field, enhance nonlinearity, and promote interactions between all the comb modes. On the one hand, a large Q/V ratio enables experiments to access exotic nonlinear regimes [3,4] and realize octave-spanning combs for applications, including clocks [5,6] and optical-frequency synthesizers [7]. On the other hand, small V increases the sensitivity to environmental and pump-laser fluctuations, which in turn degrades the comb coherence and application performance [8,9]. Recently, a high-signal-to-noise measurement of the carrier-envelope-offset frequency ($f_{\rm ceo}$) revealed the thermal noise limit for soliton microcombs [8]. Indeed, frequency fluctuations in the soliton-microcomb repetition rate, $f_{\rm rep}$, were observed to behave according to the fundamental thermodynamic relation [10]

$$\langle \delta f_{\rm rep}^2 \rangle = |\eta_T|^2 \frac{k_B T^2}{\rho C V}, \tag{1}$$

where $\langle \delta f_{\rm rep}^2 \rangle$ is the variance of $f_{\rm rep}$ frequency fluctuations, $\eta_T = df_{\rm rep}/dT$, k_B is Boltzmann's constant, T is the microresonator modal temperature, ρ is the material density, and C is the specific heat. Hence, understanding η_T is crucial for interpreting thermal noise and how soliton microcombs interact with their environment.

Here, we present a comprehensive set of predictions and measurements on controlling thermal noise in soliton microcombs, and we reveal unique behaviors of thermal-noise correlations mapped to nonlinear light propagation. Since the soliton comb modes are phase locked, they collectively respond to extrinsic properties dictated by the resonator, such as group-velocity dispersion (GVD or dispersion) and temperature. Hence, transduction of thermal fluctuations to $f_{\rm rep}$ fluctuations through η_T is coupled to how the soliton is influenced by dispersion, which is readily controlled in integrated-photonics resonators. We present an experimental validation of our predictions, which is universally applicable to soliton microcombs. With a single resonator device, we observe that the thermal-noise-limited $f_{\rm rep}$ phase noise varies significantly with the pump-laser frequency, ν_p. Finally, we investigate the impact of these physics on $f_{\rm ceo}$; our simulations indicate that spectrally similar, octave-spanning soliton microcombs may feature significant differences in their thermal-noise-limited linewidth.

Temperature induces strong correlations in soliton microcombs (Fig. 1), particularly the transduction of thermal noise to $f_{\rm rep}$ that is quantified by η_T. Figure 1(a) shows how the thermo-optic effect connects $f_{\rm rep}$ to the microresonator temperature, T, according to

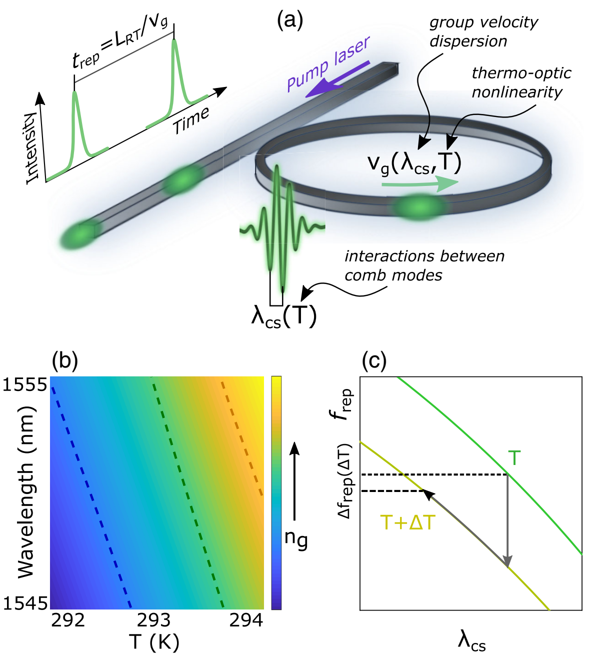

FIG. 1. (a) The soliton velocity, v_g, depends on both its wavelength, λ_{cs}, due to group-velocity dispersion (GVD), and the modal temperature, T, due to the thermo-optic effect. Hence, the pulse-to-pulse timing, $t_{rep} = 1/f_{rep}$, is sensitive to T. (b) GVD curves with T dependence. Dashed lines are lines of constant n_g. (c) Trajectory of f_{rep} for a change in T, ΔT. The GVD curve shifts due to the thermo-optic effect (vertical arrow), and the correlated change in λ_{CS} moves f_{rep} along its GVD curve (arrow parallel to curve). The change in f_{rep}, Δf_{rep}, is the total vertical displacement.

$$f_{rep}(\lambda_{CS}, T) = \frac{v_g(\lambda_{CS}, T)}{L_{RT}} = \frac{c}{n_g(\lambda_{CS}, T)L_{RT}}, \qquad (2)$$

where λ_{CS} is the wavelength of the soliton carrier wave, v_g is the soliton group velocity, L_{RT} is the microresonator circumference, c is the speed of light in vacuum, and n_g is the group refractive index that depends on both λ_{CS} due to group-velocity dispersion (GVD) and T due to the thermo-optic effect [Fig. 1(b)]. (In our analysis, we do not consider thermomechanical effects that couple L_{RT} to T. While this approximation is justified [11], thermomechanical effects can be included in our model and would not impact our conclusions). Importantly, we discover that optical nonlinearity and GVD couple λ_{CS} to T, as depicted in Fig. 1(a), and we note that such effects are unique to nonlinear, multimode optical systems. Figure 1(c) offers a graphical interpretation of η_T and depicts two GVD curves at temperatures T and $T + \Delta T$. A temperature fluctuation, ΔT, vertically displaces the GVD curve according to the material thermo-optic coefficient. Simultaneously, the correlated change in λ_{CS} causes f_{rep} to move along its new GVD curve. Hence, η_T is calculated from the total vertical displacement, Δf_{rep}, divided by ΔT, for small ΔT. In the next section, we apply simulation techniques to make these concepts more precise.

We model the temperature-dependent intraresonator field, ψ, using the Lugiato-Lefever equation (LLE) [12,13], including self-steepening (SS) and an approximation [14] for stimulated Raman scattering (SRS),

$$\frac{\partial\psi}{\partial t} = F - (1 + i\alpha)\psi - i\mathcal{D}\tilde{\psi} + \left(i + (\theta_k - i\theta_R)\frac{\partial}{\partial\theta}\right)|\psi|^2\psi, \qquad (3)$$

where F^2 is the normalized pump-laser power, $\alpha(T) = 2/\Gamma \times [\nu_0(T) - \nu_p]$ is the temperature-dependent detuning between the pump-laser frequency, ν_p, and the microresonator mode frequency, $\nu_0(T)$, that is normalized to the modal linewidth, Γ; $\mathcal{D}(\mu, T) = 2/\Gamma \times (\nu_\mu(T) - \nu_0(T) - \mu D_1/2\pi)$ is the temperature-dependent microresonator dispersion, where μ is the mode number with respect to ν_0 and $D_1/2\pi$ is the microresonator free-spectral range (FSR); $\tilde{\psi}$ represents that operations to the intraresonator field are performed in the frequency domain; θ_k and θ_R are coefficients related to SS and SRS, respectively; and $\theta = \tau D_1$ is a fast-time variable corresponding to the intraresonator angle in a moving reference frame. To calculate θ_k and θ_R, we used the values 0.13, 1.8 fs, and 1.9 fs for the Raman fraction, Raman shock time, and Kerr shock time, respectively [15,16]. Only the instantaneous Raman response is included in the model [14]. Furthermore, we distinguish the temperature-dependent dispersion, $\mathcal{D}$, from the integrated dispersion, $D_{int} = 2\pi \times (\nu_\mu - \nu_0 - \mu D_1/2\pi) = \sum_{j\geq 2} D_j\mu^j/j!$, and calculate $\nu_\mu(T)$ to first order as

$$\nu_\mu(T) = \nu_\mu(T_0) + (T - T_0)\frac{d\nu_\mu}{dT} = \nu_\mu(T_0) - (T - T_0) \times \eta_\nu \frac{\nu_\mu^2(T_0)L_{RT}}{(\mu + m)c}, \qquad (4)$$

where $\eta_\nu = dn_p/dT$ is the material thermo-optic coefficient for the refractive index, n_p, m is the mode number corresponding to ν_0, and $\nu_\mu(T_0)$ are defined by D_{int} and $\nu_0(T_0)$. We calculate f_{rep} directly from our LLE simulations by monitoring the soliton position in the moving reference frame; however, an insightful approximation for f_{rep} is given by

$$2\pi f_{rep} = \frac{2\pi(\nu_1 - \nu_{-1})}{2} + \Omega\frac{D_2}{D_1}, \qquad (5)$$

where $\Omega = 2\pi \times (\nu_{CS} - \nu_p)$ is the detuning-dependent shift of the soliton carrier-wave frequency, $\nu_{CS} = c/\lambda_{CS}$, that corresponds to asymmetry in the comb spectrum around ν_p. In general, asymmetries arise from GVD, SRS, and spectral recoil from dispersive waves (DWs) or mode crossings [17].

Hence, temperature shifts induce a response in the comb spectrum, $\Omega(T)$ or $\lambda_{\mathrm{CS}}(T)$, that is tunable through the microresonator GVD. To mitigate thermal noise, the GVD should be designed to optimize $\Omega(T)$ so that the two terms in Eq. (5) have opposite temperature dependence.

In Fig. 2 we explore the fundamental connection between GVD and thermal noise. We simulate single-soliton microcombs for fixed ν_p, F^2, and D_2, while varying D_3. We choose to vary D_3 because it is the lowest-order term in the D_{int} expansion that gives rise to spectral asymmetry, the degree of which is determined primarily by the ratio D_3/D_2. First, we sweep the temperature, T, from 293.05 to 292.95 K and monitor f_{rep}, as shown in Fig. 2(a). With $D_3 = 0$, the f_{rep} tuning is dominated by SRS, which is known to exhibit $df_{\mathrm{rep}}/d\alpha < 0$ [18]; here this manifests as large $\eta_T > 0$. As D_3 is increased from zero, η_T decreases and eventually becomes negative. From these data and for specific values of T we can calculate η_T and compare the value $|\eta_T|^2(k_B T^2/\rho C V)$ to the simulated noise variance, $\langle \delta f_{\mathrm{rep}}^2 \rangle$; see Fig. 2(c). Discrepancies between these two calculations indicate the importance of higher-order corrections to η_T [i.e., it quantifies contributions to η_T stemming from the curvature of the data in Fig. 2(a)]. To calculate $\langle \delta f_{\mathrm{rep}}^2 \rangle$ and gain a more comprehensive picture of thermal noise, we simulate the noise power spectral density of f_{rep} frequency fluctuations, S_{rep}, by including temperature within our model as a stochastic variable, subject to fluctuation dissipation

$$\dot{T} = -\Gamma_T \Delta T + \zeta_T, \tag{6}$$

where Γ_T is the thermal dissipation rate and ζ_T is a fluctuation source defined by its autocorrelation, $\langle \zeta_T(t)\zeta_T(t+\tau)\rangle = [(2\Gamma_T k_B T^2)/\rho C V]\delta(\tau)$, where $\delta(\tau)$ is the Dirac δ function [19]. Remarkably, for the same magnitude of thermal noise present in the microresonator, we observe a > 50 dB suppression of f_{rep} frequency fluctuations, as shown in Fig. 2(d). Such unprecedented flexibility in the thermal noise limit is a direct result of the nonlinear, multimode nature of soliton microcombs.

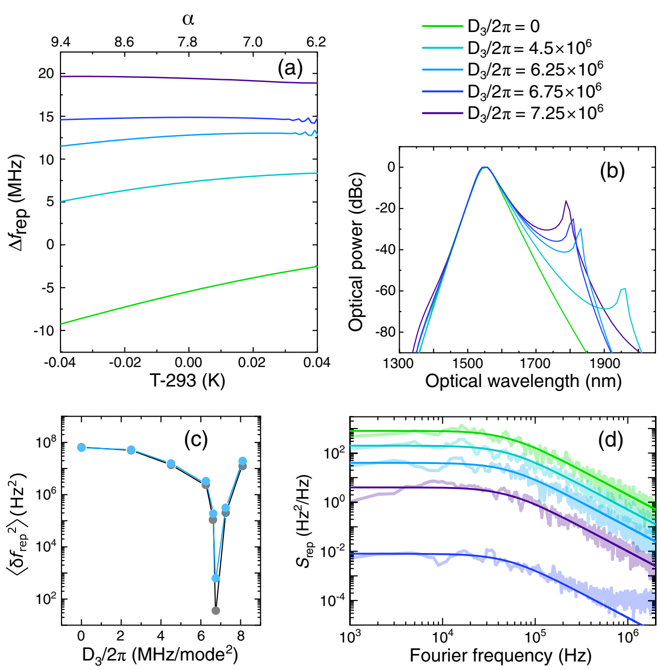

FIG. 2. LLE simulations of η_T and soliton-microcomb thermal noise for various GVD settings. Parameters for the simulations are $D_2/2\pi = 60$ MHz/mode and $F^2 = 10$. (a) Simulated f_{rep} versus T. As D_3 is increased from zero, η_T decreases and eventually becomes negative. At the lowest values of α, ripples in the data arise from small-amplitude breathing oscillations. (b) Optical spectra for various D_3. (c) Variance of f_{rep} frequency fluctuations, $\langle \delta f_{\mathrm{rep}}^2 \rangle$, calculated in two ways: From the slopes in (a) at $\alpha = 7.65$ (gray data points) and by integrating S_{rep} (blue data points). (d) Simulated S_{rep} spectra for various D_3. Faded lines are LLE simulation results, and bold lines are fits to the data. The effective noise floor of our simulations is 10^{-4} $\mathrm{Hz}^2/\mathrm{Hz}$.

We perform experiments to test our modeling and predictions, using a single soliton circulating a Si_3N_4 (SiN) microresonator at a rate $f_{\mathrm{rep}} \approx 1$ THz; the optical spectrum is pictured in Fig. 3(a). We measure f_{rep} by electro-optic modulation [6], as shown in Figs. 3(b) and 3(c). We confirm a thermal-noise-limited f_{rep} signal by ruling out fluctuations of both the pump-laser frequency and intensity [8] and by comparing our measurements to a thermal noise model [20]. In our experiments, we cannot accurately control the modal temperature; therefore, we record f_{rep} versus ν_p [Fig. 3(d)] and understand η_T through the decomposition

$$\eta_T = \frac{d\nu_0}{dT}\frac{df_{\mathrm{rep}}}{d\nu_0} = \frac{d\nu_0}{dT}\left(\frac{\partial f_{\mathrm{rep}}}{\partial \nu_0} + \frac{2}{\Gamma}\frac{\partial f_{\mathrm{rep}}}{\partial \alpha}\right), \tag{7}$$

where the partial derivative with respect to ν_0 (α) indicates that α (ν_0) is held fixed. Equation (7) explicitly separates the contributions to η_T traced back to Fig. 1(c); specifically, $d\nu_0/dT \times \partial f_{\mathrm{rep}}/\partial \nu_0 = d\mathrm{FSR}/dT$ corresponds to the vertical black arrow, while $d\nu_0/dT \times (2/\Gamma)(\partial f_{\mathrm{rep}}/\partial \alpha)$ corresponds to the other arrow. Moreover, Eq. (7) points to measurement steps for predicting η_T without knowing the microresonator dispersion, impact of mode crossings, etc. For our measurements we approximate that $(\Gamma/2)(d\alpha/d\nu_p) \approx -1$, which is generally valid for large α [21]. Moreover, $d\nu_0/dT \approx -2.5$ GHz/K for SiN microresonators [8,22] and $\partial f_{\mathrm{rep}}/\partial \nu_0 \approx 1/m$ [23]. Hence, we estimate η_T from our measurements as $-2.5\ \mathrm{GHz/K}(5.2\ \mathrm{MHz/GHz} - df_{\mathrm{rep}}/d\nu_p)$. Importantly, Eq. (7) predicts that for a thermal-noise-limited f_{rep} signal, operating near $df_{\mathrm{rep}}/d\nu_p = 0$ does not yield the lowest noise as for previous observations of so-called quiet points [17]. Rather, the thermal noise will be mitigated when $2/\Gamma(\partial f_{\mathrm{rep}}/\partial \alpha) \approx -\partial f_{\mathrm{rep}}/\partial \nu_0$, which physically corresponds to a balance between thermal changes in the FSR with thermal changes in Ω [i.e., a balance in the

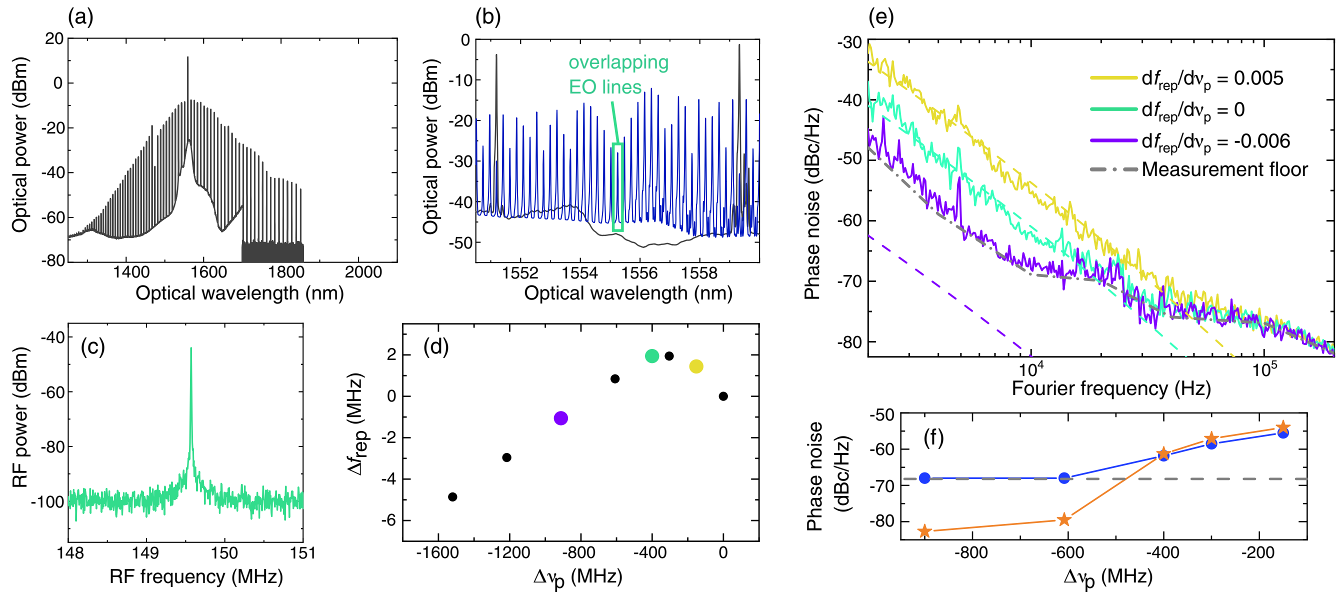

FIG. 3. Experimental evidence for thermal-noise mitigation by a balance of thermal shifts in GVD and Ω. (a) Optical spectrum used in the experiments. (b) Repetition frequency ($f_{\rm rep}$) detection by electro-optic modulation. The soliton-microcomb spectrum is shown both before electro-optic modulation (black) and after (blue). (c) Radio frequency spectrum (1 kHz resolution bandwidth) of the thermal-noise-limited $f_{\rm rep}$ signal. (d) $f_{\rm rep}$ versus ν_p. These data are used to estimate η_T and predict $S_{\rm rep}$. (e) $S_{\rm rep}$ phase-noise measurements of the 1-THz repetition rate for various settings of ν_p. Dashed lines correspond to predictions from our thermal noise model using η_T estimates from (d). (f) $S_{\rm rep}$ measurements at 10 kHz offset (blue circles) and predictions based on Eq. (7) and our thermal-noise model (orange stars). The dashed gray line corresponds to our measurement floor.

two terms of Eq. (5)]. Guided by Eq. (7), we estimate η_T values for the purple, green, and gold data points as 0.8, -13, and -30 MHz/K, respectively. Our phase-noise measurements are consistent with these values and show ≈15 dB of noise suppression for the different settings of ν_p, but the lowest-noise data is limited by our measurement floor, which is set by the synthesizer used to drive the electro-optic modulators for $f_{\rm rep}$ detection. Our phase-noise measurements agree with a thermal-noise model, shown by the dashed lines in Fig. 3(e). The model uses our measurements of η_T and multiplies them by an expression for microresonator thermorefractive noise [20]. Based on our estimations of η_T, we expect that $f_{\rm rep}$ frequency fluctuations are suppressed by almost 30 dB when operating at $\Delta\nu_p = 900$ MHz (purple data) compared to $\Delta\nu_p = 180$ MHz (gold data). We emphasize that, in general, accurate predictions of η_T based on Eq. (7) will require measuring $df_{\rm rep}/d\alpha$ without approximations, and that here our primary goal was to verify the connection between Eq. (7) and thermal noise. Our measurements confirm that thermal noise in soliton microcombs is not a rigid limit set by material properties, but instead arises from complex interactions between many microcomb modes as determined by optical nonlinearity (especially SRS) and GVD.

Finally, we model the impact of thermal noise on octave-spanning soliton microcombs and emphasize its role in $f_{\rm ceo}$ detection. First, we assess that D_3 plays the primary role in coupling $D_{\rm int}$ to η_T; therefore, we model two spectrally similar, octave-spanning solitons with $D_3/2\pi$ values of 0 and 1.5×10^6 MHz/mode^2, respectively. $D_{\rm int}$ curves and optical spectra for each comb are shown in Figs. 4(a) and 4(b), respectively. To approximately match the DW locations, we manipulate higher-order dispersion terms in the LLE. Importantly, for spectrally broad solitons featuring strong DWs, DW recoil, and soliton self-interactions can significantly impact η_T [24]. In our simulations, we have tried to avoid this regime by operating at low F^2, but note that understanding these effects will be important for future experiments. In Fig. 4, we present simulation results comparing the two soliton microcombs. Despite having similar optical spectra, $\eta_T \approx 130$ MHz/K for the $D_3 = 0$ comb (hereafter referred to as the noisy comb), indicating that SRS primarily controls the $f_{\rm rep}$ tuning, while $\eta_T \approx 0$ for the $D_3/2\pi = 1.5\times10^6$ comb (hereafter referred to as the quiet comb), as shown in Fig. 4(c). These dynamics are in agreement with the simpler combs analyzed in Fig. 2. Unsurprisingly, we observe a > 50 dB difference in the $S_{\rm rep}$ spectra of the two combs. To understand the implications for $f_{\rm ceo}$, we calculate the noise power spectral density of $f_{\rm ceo}$ frequency fluctuations, $S_{\rm ceo}$, as $S_{\rm ceo} = m^2 \times S_{\rm rep}$; the resulting spectra are shown in Fig. 4(e). These data have important implications for soliton-microcomb applications. For example, by comparing each spectrum with the beta line [25], we assess that stabilization of the soliton microcombs for coherent applications [26] would require ≈700 kHz of servo bandwidth for the noisy comb (in

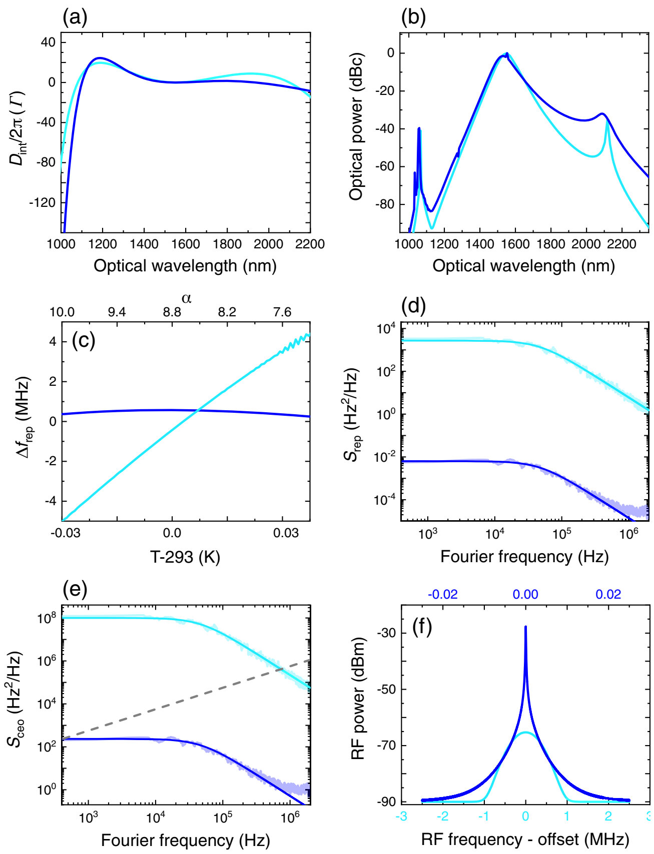

FIG. 4. Simulations of thermal noise in octave-spanning soliton microcombs. (a) D_{int} for the two solitons analyzed in this study. Parameters for the dark blue traces (units omitted): $D_2/2\pi = 20 \times 10^6$, $D_3/2\pi = 1.5 \times 10^6$, $D_4/2\pi = -52 \times 10^3$, $D_5/2\pi = -4 \times 10^3$, $F^2 = 12$, $\alpha = 9.3$. Parameters for the light blue traces: $D_2/2\pi = 20 \times 10^6$, $D_3/2\pi = 0$, $D_4/2\pi = -120 \times 10^3$, $D_5/2\pi = 5.3 \times 10^3$, $D_6/2\pi = -150$, $F^2 = 12$, $\alpha = 9.25$. (b) Optical spectra corresponding to the dispersion profiles in (a). (c) f_{rep} versus T. (d) S_{rep} spectra. (e) S_{ceo} spectra calculated from $m^2 \times S_{\mathrm{rep}}$. The dashed line is the so-called beta line for understanding which Fourier frequencies contribute to the signal linewidth. (f) Simulated f_{ceo} beat note that indicates both coherence and signal-to-noise ratio are improved by mitigating thermal noise. The top (bottom) axis refers to the blue (cyan) trace.

addition to significantly greater gain for overcoming the excess noise) but only ≈400 Hz of bandwidth for the quiet comb. Moreover, we integrate the spectra from Fig. 4(e) and apply the Wiener-Khintchine theorem to analyze the f_{ceo} beat note, shown in Fig. 4(f). We make two noteworthy observations: first, the thermal-noise-limited linewidths for the noisy and quiet combs are approximately 1 MHz and 100 Hz, respectively. Second, the signal-to-noise ratios for the noisy and quiet combs are approximately 25 and 60 dB, respectively. Both of these measures impact applications requiring low noise and good optical coherence.

In conclusion, soliton microcombs offer a unique lens through which to view thermodynamic processes and noise. We have shown how interactions between comb modes induce thermodynamic correlations that may be harnessed to manipulate the thermal noise limit. Our results shed light on the relationship between nonlinear physics in multimode systems and the intrinsic, microscopic fluctuations therein.

We thank Jizhao Zang and Su Peng Yu for a careful reading of the Letter, and Ligentec for fabricating the device used in experiments. This project is funded by the DARPA DRINQS program.

*jordan.stone@colorado.edu

[1] T. Fortier and E. Baumann, Commun. Phys. **2**, 153 (2019).
[2] T. J. Kippenberg, A. L. Gaeta, M. Lipson, and M. L. Gorodetsky, Science **361**, eaan8083 (2018).
[3] D. C. Cole, E. S. Lamb, P. DelHaye, S. A. Diddams, and S. B. Papp, Nat. Photonics **11**, 671 (2017).
[4] M. Anderson, Y. Wang, F. Leo, S. Coen, M. Erkintalo, and S. G. Murdoch, Phys. Rev. X **7**, 031031 (2017).
[5] Z. Newman, V. Maurice, T. Drake, J. Stone, T. Briles, D. Spencer, C. Fredrick, Q. Li, D. Westly, B. Ilic *et al.*, Optica **6**, 680 (2019).
[6] T. E. Drake, T. C. Briles, J. R. Stone, D. T. Spencer, D. R. Carlson, D. D. Hickstein, Q. Li, D. Westly, K. Srinivasan, S. A. Diddams, and S. B. Papp, Phys. Rev. X **9**, 031023 (2019).
[7] T. C. Briles, J. R. Stone, T. E. Drake, D. T. Spencer, C. Fredrick, Q. Li, D. Westly, B. Ilic, K. Srinivasan, S. A. Diddams *et al.*, Opt. Lett. **43**, 2933 (2018).
[8] T. E. Drake, J. R. Stone, T. C. Briles, and S. B. Papp, arXiv:1903.00431.
[9] J. Liu, E. Lucas, A. S. Raja, J. He, J. Riemensberger, R. N. Wang, M. Karpov, H. Guo, R. Bouchand, and T. J. Kippenberg, Nat. Photonics **14**, 486 (2020).
[10] L. D. Landau, and E. M. Lifshitz, Statistical Physics (Elsevier, 2013), Vol. **5**.
[11] A. B. Matsko, A. A. Savchenkov, N. Yu, and L. Maleki, J. Opt. Soc. Am. B **24**, 1324 (2007).
[12] S. Coen, H. G. Randle, T. Sylvestre, and M. Erkintalo, Opt. Lett. **38**, 37 (2013).
[13] Y. K. Chembo and C. R. Menyuk, Phys. Rev. A **87**, 053852 (2013).
[14] M. Karpov, H. Guo, A. Kordts, V. Brasch, M. H. P. Pfeiffer, M. Zervas, M. Geiselmann, and T. J. Kippenberg, Phys. Rev. Lett. **116**, 103902 (2016).
[15] C. Bao, Y. Xuan, C. Wang, J. A. Jaramillo-Villegas, D. E. Leaird, M. Qi, and A. M. Weiner, Opt. Lett. **42**, 759 (2017).
[16] C. Bao, L. Zhang, L. C. Kimerling, J. Michel, and C. Yang, Opt. Express **23**, 18665 (2015).
[17] X. Yi, Q.-F. Yang, X. Zhang, K. Y. Yang, X. Li, and K. Vahala, Nat. Commun. **8**, 14869 (2017).
[18] X. Yi, Q.-F. Yang, K. Y. Yang, and K. Vahala, Opt. Lett. **41**, 3419 (2016).
[19] X. Sun, R. Luo, X.-C. Zhang, and Q. Lin, Phys. Rev. A **95**, 023822 (2017).

[20] N. Kondratiev and M. Gorodetsky, Phys. Lett. A **382**, 2265 (2018).

[21] J. R. Stone, T. C. Briles, T. E. Drake, D. T. Spencer, D. R. Carlson, S. A. Diddams, and S. B. Papp, Phys. Rev. Lett. **121**, 063902 (2018).

[22] G. Huang, E. Lucas, J. Liu, A. S. Raja, G. Lihachev, M. L. Gorodetsky, N. J. Engelsen, and T. J. Kippenberg, Phys. Rev. A **99**, 061801(R) (2019).

[23] X. Xue, Y. Xuan, C. Wang, P.-H. Wang, Y. Liu, B. Niu, D. E. Leaird, M. Qi, and A. M. Weiner, Opt. Express **24**, 687 (2016).

[24] D. Skryabin and Y. Kartashov, Opt. Express **25**, 27442 (2017).

[25] G. Di Domenico, S. Schilt, and P. Thomann, Appl. Opt. **49**, 4801 (2010).

[26] D. R. Carlson, D. D. Hickstein, W. Zhang, A. J. Metcalf, F. Quinlan, S. A. Diddams, and S. B. Papp, Science **361**, 1358 (2018).